Draft version January 19, 2016
Preprint typeset using LaTeX style emulateapj v. 5/2/11

arXiv:1511.01434v2 [astro-ph.HE] 18 Jan 2016

EFFICIENT PRODUCTION OF HIGH-ENERGY NONTHERMAL PARTICLES DURING MAGNETIC RECONNECTION IN A MAGNETICALLY-DOMINATED ION-ELECTRON PLASMA

Fan Guo[1], Xiaocan Li[1,2], Hui Li[1], William Daughton[1], Bing Zhang[3], Nicole Lloyd-Ronning[1], Yi-Hsin Liu[4], Haocheng Zhang[1], Wei Deng[1,3]

Draft version January 19, 2016

ABSTRACT

Magnetic reconnection is a leading mechanism for dissipating magnetic energy and accelerating nonthermal particles in Poynting-flux dominated flows. In this letter, we investigate nonthermal particle acceleration during magnetic reconnection in a magnetically-dominated ion-electron plasma using fully kinetic simulations. For an ion-electron plasma with the total magnetization $\sigma_0 = B^2/(4\pi n(m_i + m_e)c^2)$, the magnetization for each species is $\sigma_i \sim \sigma_0$ and $\sigma_e \sim (m_i/m_e)\sigma_0$, respectively. We have studied the magnetically dominated regime by varying $\sigma_e = 10^3 - 10^5$ with initial ion and electron temperatures $T_i = T_e = 5 - 20 m_e c^2$ and mass ratio $m_i/m_e = 1 - 1836$. The results demonstrate that reconnection quickly establishes power-law energy distributions for both electrons and ions within several $(2-3)$ light-crossing times. For the cases with periodic boundary conditions, the power-law index is $1 < s < 2$ for both electrons and ions. The hard spectra limit the power-law energies for electrons and ions to be $\gamma_{be} \sim \sigma_e$ and $\gamma_{bi} \sim \sigma_i$, respectively. The main acceleration mechanism is a Fermi-like acceleration through the drift motions of charged particles. When comparing the spectra for electrons and ions in momentum space, the spectral indices s_p are identical as predicted in Fermi acceleration. We also find that the bulk flow can carry a significant amount of energy during the simulations. We discuss the implication of this study in the context of Poynting-flux dominated jets and pulsar winds especially the applications for explaining the nonthermal high-energy emissions.

Subject headings: acceleration of particles — magnetic reconnection — relativistic processes — gamma-ray bursts: general — galaxies: jets — pulsars: general

1. INTRODUCTION

It is thought that magnetic field is of central importance in pulsar wind nebulae (PWNe) and jets from active galactic nuclei (AGNs) and gamma-ray bursts (GRBs). The initially launched relativistic flows are Poynting-flux dominated (Spruit 2010). Meanwhile, these astrophysical phenomena are observed to have nonthermal spectra that arise from various emission processes of energetic particles. For example, leptonic modeling of TeV blazar emissions requires a power-law electron distribution with energy $\gamma_e \sim 10^3 - 10^5$ (Böttcher et al. 2013). The spectra of gamma-ray bursts during the prompt phase suggest that the radiating particles have Lorentz factors $\gamma_e \sim 10^3 - 10^7$ (Daigne & Mochkovitch 1998; Uhm & Zhang 2014). In hadronic models, protons also need to be accelerated to high energies and may be related to ultra-high-energy cosmic rays (Böttcher et al. 2013). Understanding how the energy stored in magnetic fields being converted into nonthermal particle energy is essential to interpret observed emissions in those high-energy astrophysical processes.

Recent studies of GRBs (Zhang & Yan 2011; McKinney & Uzdensky 2012; Kumar & Crumley 2015), AGNs (Giannios et al. 2009; Zhang et al. 2015a) and PWNe (Uzdensky & Spitkovsky 2014) have shown that models that are magnetically dominant can explain much of the observed data. It is estimated that the magnetization parameter $\sigma \equiv B^2/(4\pi w)$ can be large and the Alfvén speed approaches the light speed $v_A \sim c$. Here B is the magnitude of magnetic field and w is the enthalpy. To explain the observed high-energy emissions, an efficient conversion from energies in the magnetized flow into nonthermal particles is required (e.g., Zhang & Yan 2011). Collisionless shocks that are considered to be efficient for particle acceleration in weakly magnetized plasmas are inefficient in dissipating energy and accelerating nonthermal particles in magnetically-dominated flows (Sironi et al. 2015; Zhang et al. 2015b).

Magnetic reconnection is a major candidate that unleashes magnetic energy in magnetized flows through reorganizing magnetic topology (Zweibel & Yamada 2009). In the relativistic limit, the magnetic energy gets strongly dissipated in the reconnection region (Blackman & Field 1994; Lyutikov & Uzdensky 2003; Comisso & Asenjo 2014; Liu et al. 2015).

Theory of nonthermal particle acceleration in reconnection layers is still evolving (de Gouveia dal Pino & Lazarian 2005; Drake et al. 2006; Drury 2012; Guo et al. 2014; Zank et al. 2014). Much progress has been made through particle-in-cell (PIC) kinetic simulations that self-consistently model the microscopic physics of collisionless reconnection and nonthermal plasma energization. Earlier studies focus on the low-σ regime ($\sigma < 1$), and identified several basic acceleration mechanisms such

guofan.ustc@gmail.com
[1] Los Alamos National Laboratory, Los Alamos, NM 87545, USA
[2] Department of Space Sciences, University of Alabama in Huntsville, Huntsville, AL 35899, USA
[3] Department of Physics and Astronomy, University of Nevada Las Vegas, Las Vegas, NV 89154, USA
[4] NASA Goddard Space Flight Center, Greenbelt, MD 20771, USA
[5] Astrophysical Institute, Department of Physics and Astronomy, Ohio University, Athens, OH 45701, USA

as direct acceleration at X-lines (Fu et al. 2006; Huang et al. 2010), Fermi-type acceleration associated with plasmoids (Drake et al. 2006), and further acceleration in plasmoid coalescence regions (Oka et al. 2010). Simulations with mildly relativistic parameters ($\sigma \sim 1$) have uncovered particle acceleration with power-law energy spectra in X-lines (Zenitani & Hoshino 2001; Bessho & Bhattacharjee 2012), but no significant power-law distribution when the spectra are integrated over the whole domain (Zenitani & Hoshino 2007; Liu et al. 2011; Kagan et al. 2013). Recently, there is an explosion of studies on relativistic magnetic reconnection in the magnetically-dominated regime ($\sigma \gg 1$) (Cerutti et al. 2012; Sironi & Spitkovsky 2014; Guo et al. 2014, 2015; Melzani et al. 2014b; Werner et al. 2014; Liu et al. 2015), primarily motivated by the discovery of the spectacular Crab flares (Abdo et al. 2011; Tavani et al. 2011) and development of the magnetically-dominated models. Several simulations have reported hard power-law distributions with spectral index $1 \leq s \leq 2$ when $\sigma \gg 1$ (Sironi & Spitkovsky 2014; Guo et al. 2014, 2015; Melzani et al. 2014b; Werner et al. 2014) **. These new simulations claim power-law distributions in the whole reconnection region, suggesting reconnection in the magnetically-dominated regime may be a strong source of nonthermally particles. Guo et al. (2014, 2015) used a force-free current sheet that does not require the hot plasma population in a Harris sheet and showed that the energy spectra of particles within the entire reconnection layer resembles a power law. Through calculating the guiding-center drift motions of all the simulated particles, we have demonstrated that the primary acceleration mechanism is a first-order Fermi mechanism resulting from the particle curvature drift motion along the direction of the $-\mathbf{v} \times \mathbf{B}/c$ electric field induced by the relativistic flows. The acceleration leads to the formation of hard power-law spectra $f \propto (\gamma - 1)^{-s}$ with $s \sim 1$ for sufficiently strong magnetic field and large simulation domains. We have developed an analytical model to describe the simulation results and derived a general condition for the formation of the power-law distributions, i.e., the acceleration time scale needs to be shorter than the time scale for particles injected into the reconnection region $\tau_{acc} < \tau_{inj}$. The solution may also explain simulations from the Harris current layer (Sironi & Spitkovsky 2014; Melzani et al. 2014b; Werner et al. 2014). The power-law distribution has also been found in nonrelativistic reconnection simulations with a low-β ($\beta = 8\pi nkT/B^2 \ll 1$) plasma (Li et al. 2015), showing the mechanism can be applied in a larger parameter range.

Most PIC simulations of relativistic magnetic reconnection focused on pair plasmas. In general the plasma composition is uncertain and can be either electron-positron pairs or electron-ion plasmas. While proton-electron reconnection has been studied by Melzani et al. (2014a,b) with a limited parameter range ($m_i/m_e = 1 - 50$, $\sigma_0 = B^2/4\pi(m_i + m_e)nc^2 = 1 - 10$), here we show results from two-dimensional PIC simulations for a magnetically dominated ion-electron plasma, the magnetization for each species is $\sigma_i \sim \sigma_0$ and $\sigma_e \sim (m_i/m_e)\sigma_0$. We study the magnetically dominated regime for a range of σ_0 with different ion and electron temperatures and mass ratio m_i/m_e up to 1836. We demonstrate that reconnection quickly establishes power-law distributions for both electrons and ions within several light-crossing times. The power-law index is $1 < s < 2$ for both electrons and ions in the cases with periodic boundaries. The break energies for electrons and ions are $\gamma_{be} \sim \sigma_e$ and $\gamma_{bi} \sim \sigma_i$. For the antiparallel case we study, the main acceleration mechanism for particles in the power-law is a Fermi-like acceleration through drift motions of charged particles, consistent with earlier work (Guo et al. 2014, 2015). The numerical methods are presented in Section 2. Section 3 discusses the main results of the paper. In Section 4, we discuss the implications of the study in the context of high-energy astrophysics. Our conclusions are summarized in Section 5.

** Several papers reported $s > 2$ but the spectra are plotted as a function of Lorentz factor γ rather than kinetic energy $\gamma - 1$. When plotting energy spectrum as a function of $\gamma - 1$, we did not find obvious power-law distribution with $s > 2$ for simulations with periodic boundary conditions.

2. NUMERICAL METHODS

The simulations start from a magnetically-dominated force-free current sheet. Previous studies have shown that the intense current sheets can develop through various processes such as striped wind geometry, field-line foot-point motion, and turbulence cascade (Coroniti 1990; Titov et al. 2003; Makwana et al. 2015). The initial condition of our simulations is a force-free current layer with $\mathbf{B} = B_0 \tanh(z/\lambda)\hat{x} + B_0 \mathrm{sech}(z/\lambda)\hat{y}$(Guo et al. 2014, 2015). This corresponds to a rotating magnetic field with a 180° change in direction within a thickness of 2λ. The initial distributions are spatially uniform with density n_0 and relativistic Maxwellian in energy space. The current density $\mathbf{J} = en_0(\mathbf{U}_i - \mathbf{U}_e)$ is represented by a drift velocity $\mathbf{U}_i = -\mathbf{U}_e$ that satisfies Ampere's law.

The simulations assume an electron-ion plasma with mass ratio $m_i/m_e = 1 \rightarrow 1836$ and we mainly focus on the case with $m_i/m_e \gg 1$. For simplicity, the initial thermal temperatures for ions and electrons are assumed to be the same and varied in a range $T_i = T_e = 5 \rightarrow 20 m_e c^2$ to examine its effect on the resulting energy spectra. This temperature is similar to the temperature inferred for AGN jets (Homan et al. 2006). The full particle simulations are performed using the VPIC code (Bowers et al. 2009), which explicitly solves Maxwell equations and the relativistic equation of motion for the particles. In the simulations, σ_e is adjusted by changing the ratio of the nonrelativistic electron gyrofrequency $\Omega_{ce0} = eB/(m_e c)$ to the nonrelativistic electron plasma frequency $\omega_{pe0} = \sqrt{4\pi ne^2/m_e}$, $\sigma_e \equiv B^2/(4\pi n_e m_e c^2) = (\Omega_{ce0}/\omega_{pe0})^2$ and the total magnetization is $\sigma_0 \sim (m_e/m_i)\sigma_e$. We primarily discuss simulations with $\sigma_e = 10^3 \rightarrow 10^5$. The cell sizes are chosen so $\Delta x = \Delta z < 0.1 d_e$. Here $d_e = \sqrt{\gamma_0} d_{e0}$, in which $\gamma_0 = 1 + 3T_e/2m_e c^2$ and $d_{e0} = c/\omega_{pe0}$. All the simulations have 100 electron-ion pairs in each cell. Similar to numerous earlier studies, the boundary conditions in the x-direction are periodic for both fields and particles, and in the z-direction the boundaries are conductive for the field and reflect particles when they reach the boundaries. A long-wavelength perturbation with $B_z = 0.05 B_0$ is included to initiate reconnection. To ensure numerical convergence, it is essential to have enough particles per cell and spatial grids to avoid excessive numerical heating (Guo et al. 2015). We have monitored

the numerical energy conservation to ensure that effect does not influence our results. A more comprehensive study will be reported in another publication (Guo et al. 2016 in preparation).

3. SIMULATION RESULTS

Figure 1 shows the current layer evolution in the simulation with $\sigma_e = 10^4$, $T_i = T_e = 10 m_e c^2$, and $m_i/m_e = 100$ so $\sigma_0 \sim 100$. The domain size is $L_x \times L_z = 4000 d_{e0} \times 2000 d_{e0}$. This is the representative run that we will discuss in detail. The left panels and right panels show the current density and velocity in the x-direction at $\omega_{pe0} t = 2000$, 3000, and 5000, respectively. The current sheet thins down under the influence of the perturbation and then breaks into many fast-moving secondary plasmoids due to the growth of secondary tearing instability. The thinning phase lasts until $\omega_{pe0} t \sim 2000$ and rest of the simulation is dominated by the evolution of plasmoids. These plasmoids coalesce and merge into a single island on the order of the system size. The whole process is similar to the case with pair plasmas (Daughton & Karimabadi 2007) as long as the simulation domain is sufficiently large to contain several secondary tearing modes. The simulation also shows the development of fast bulk plasma flows with bulk Lorentz factors $\Gamma = 1/\sqrt{1-(V/c)^2}$, associated with plasmoids (Liu et al. 2015; Guo et al. 2015). As we will discuss below, the fast moving plasmoids contain most of the accelerated energetic particles, which likely generates high-energy nonthermal emissions with strong beaming effects. We also observed magnetosonic waves generated as the plasmoids interact with each other, similar to recent MHD simulations (Yang et al. 2015).

Figure 2 summarize the plasma energetics for the representative run. In Figure 2(a), the magnetic energy in the reconnecting component drops more than 60% within $2-3$ light crossing times and most of it gets converted into plasma energies. Ions gain slightly more energy than electrons $E_{ki}/E_{ke} \sim 1.1$. Increasing m_i/m_e to 1836, we find $E_{ki}/E_{ke} \sim 1.5$, meaning in this case the energy partition does not strongly depend on the ion-to-electron mass ratio. Figure 2(b) shows the evolution of bulk energy, internal energy, and total kinetic energy. The internal energy is defined as the kinetic energy in the local plasma frame. The bulk energy is energy associated with the plasma bulk motion. The figure shows that the bulk flow can carry a nontrivial portion of the total plasma energy during the energy conversion. Initially it exceeds the internal energy and still contains $5-10\%$ of the total kinetic energy toward the end of the simulation.

Figure 3 presents the energy spectra for both electrons and ions at different simulation times for the representative case. In energy space, electron distribution shows a power-law distribution with $s \sim 1.35$, whereas the ion distribution shows a power law with another slope $s \sim 1.2$ starting from several times of the initial thermal energy. The break energies correspond to $\gamma_{be} \sim \sigma_e$ and $\gamma_{bi} \sim \sigma_i$ and above that the spectra resemble an exponential cutoff. During the initial phase ($\omega_{pe0} t < 3000$), the flat spectrum is associated with the acceleration by the parallel electric field during the thinning process and later the acceleration is dominated by Fermi acceleration associated with plasmoid motion (see discussion below). Figure 3(c) shows the momentum distribution $f(p)p^2$ for both of the species. We find that if the two distributions are plotted in momentum space, they give almost the same slope $f(p) \propto p^{-s_p}$ and $s_p \sim 3.35$. This is a general feature of Fermi acceleration but not obviously predicted by other mechanism proposed to explain power-laws generated in reconnection regions (Sironi & Spitkovsky 2014; Werner et al. 2014).

Figure 4 compares electron energy spectra for simulations with different (a) σ_e, (b) initial temperature, (c) box size, and (d) mass ratio. Results show that for a sufficiently large domain, both electrons and ions get efficient accelerated and form a power-law distribution. For different σ_e, we observe slightly harder spectrum as the available magnetic energy increases compare to the plasma energy. The trend is similar as we reduce the thermal energy. Panel (c) shows that for a larger simulation domain, the power-law distribution becomes fully developed. As the box size increased to $L_x = 4000 d_{e0}$ for $m_i/m_e = 100$, the energy spectra are similar for larger systems. We also find that as long as the simulation domain is sufficiently large, the mass ratio does not significantly influence the electron spectrum. As for the spectral index, we find that the simulations give $1 < s < 2$ for the periodic closed system typically used for reconnection studies. This, however, may be changed for the case with open boundary conditions (Daughton et al. 2006) where the particle escape from the boundaries could lead to a softer spectrum (Guo et al. 2014, 2015).

Now we briefly discuss the acceleration of protons and electrons using a particle tracking module newly implemented in VPIC. We find that for particles initially in the current sheet, they mainly experience strong direct acceleration through parallel electric field. Typical examples for both electrons and ions are shown in Figure 5(a). For particles that get accelerated to the highest energies γ_{max} in the simulation, this is the main type of acceleration. However, for the accelerated particles that form the power-law distribution $\gamma < \gamma_b$, the main acceleration pattern is a Fermi-like process where particles gain energy by bouncing back and forth a few times associated with the motion of plasmoids as the plasmoids evolve and coalesce. In Figure 5(b) we show typical particle trajectories that resemble the Fermi mechanism. The acceleration process for both electrons and ions are very similar. We verified that the size of the largest island is well above the gyroradius of power-law ions with the real mass ratio. In a forthcoming paper, we will discuss the statistics of particle acceleration in detail similar to previous studies (Guo et al. 2014; Li et al. 2015).

4. DISCUSSION AND IMPLICATIONS

It is thought that as relativistic jets or pulsar winds are launched, initially the energy flow are magnetically dominated and then the magnetic energy gets converted into plasma energy (Spruit 2010). During this process strong sheared current sheets may form (McKinney & Uzdensky 2012) and magnetic energy gets converted into plasma energy through magnetic reconnection and produces nonthermal emission. Our results imply that the observed nonthermal emission from AGNs, GRBs, and PWNe could come from strong particle acceleration in magnetic reconnection regions. For example, when modeling the emissions from TeV blazars, it is

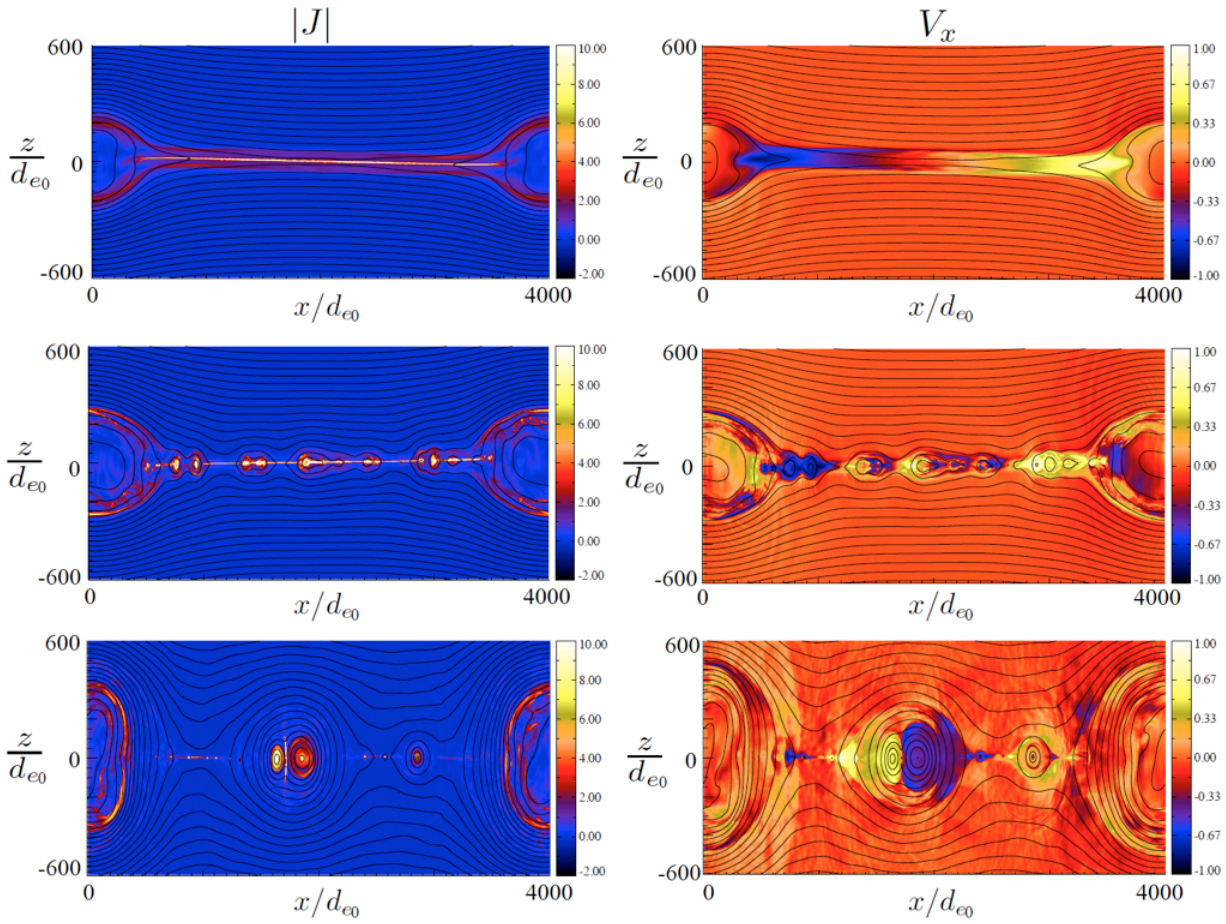

FIG. 1.— Time evolution of 2D current density and bulk flow velocity along the x-direction for the case $\sigma_0 = 100$, $m_i/m_e = 100$ at $\omega_{pe}t = 2000$, 3000, and 5000. The secondary tearing mode breaks the elongated current sheet and produce multiple plasmoids with the associated maximum bulk flow gamma of a few.

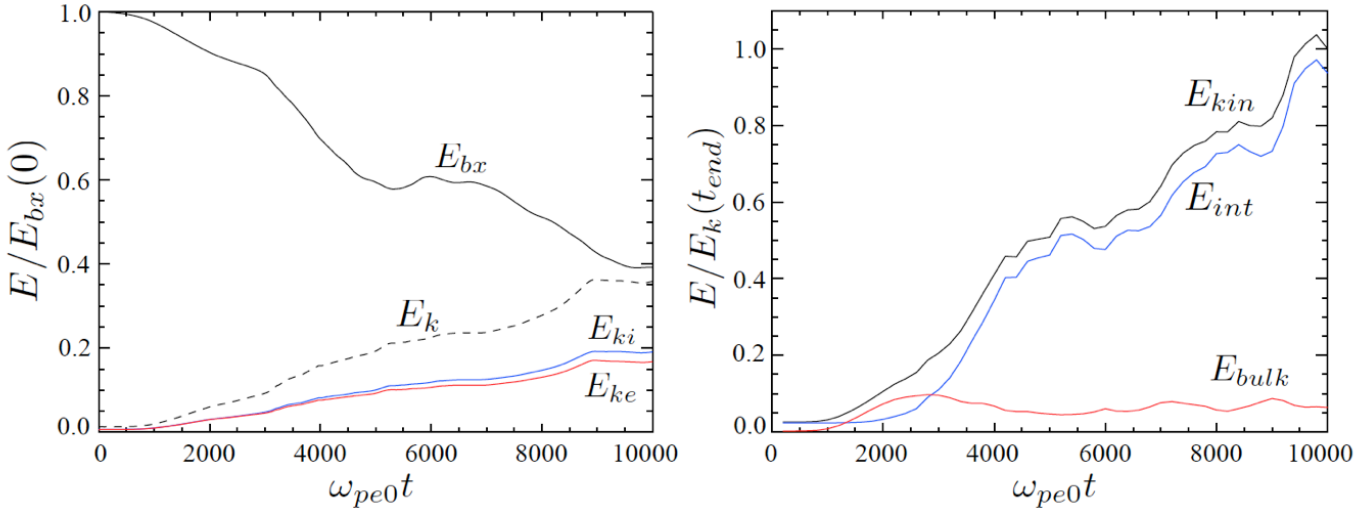

FIG. 2.— Energetics for the run with $\sigma_0 = 100$, $m_i/m_e = 100$. Left panel: evolution of reconnecting magnetic energy $B_x^2/8\pi$, ion kinetic energy and electron kinetic energy. Right panel: the evolution of total kinetic energy, internal energy, and bulk flow energy.

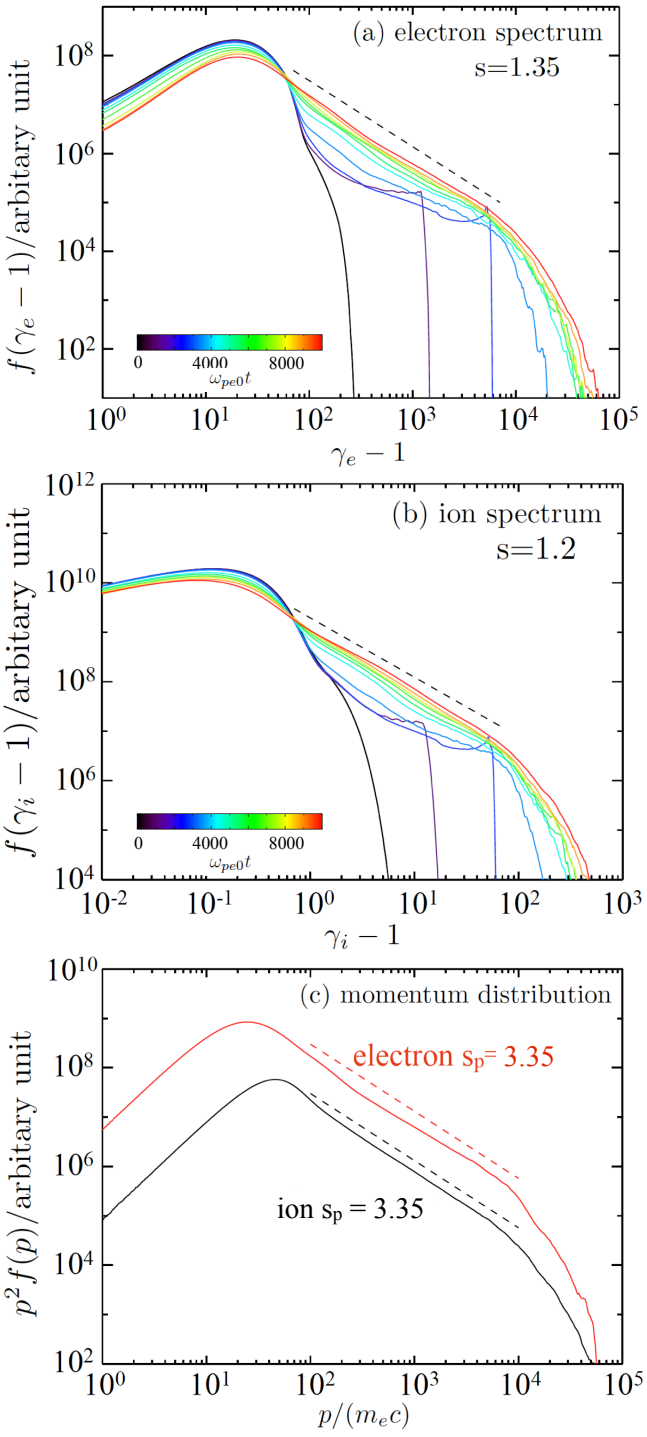

FIG. 3.— Energy distributions $f(E)$ and momentum distributions $f(p)p^2$ for both ions and electrons for the representative run with $\sigma_0 = 100$ and $m_i/m_e = 100$.

required that the electron spectrum is a power-law distribution with energy range $\gamma_e = 10^3 - 10^5$ (Böttcher et al. 2013). Recent observations show that strong multi-wavelength flares are sometimes accompanied by strong polarization variations, indicating the active participation of magnetic field during flares (Zhang et al. 2015a). Our calculation shows the development of power-law distribution with break energy $\gamma_{be} \sim \sigma_e$ regardless of the ion-to-electron mass ratio, suggesting that the nonthermal electrons can be produced when $1 \lesssim \sigma_0 \lesssim 100$ ($1800 \lesssim \sigma_e \lesssim 1.8 \times 10^5$) for real mass ratio. Our simulations show the spectral index is $1 < s < 2$, which is sometimes reported in TeV blazars (Hayashida et al. 2015; Yan et al. 2015). Most of energetic particles are contained in plasmoids and the bulk flow Lorentz factor Γ can be a few so we expect radiation from the nonthermal particles has strong beaming effects that may help explain fast variability observed in TeV blazars (Giannios et al. 2009).

In GRBs, the spectra of prompt emission suggest that the radiating electrons can reach $\gamma_e \sim 100$ and form a non-thermal energy distribution. In our simulation, the power-law distribution starts from several times of the thermal energy ($\gamma_1 \sim 50 - 200$) and extends to high energies ($\gamma_2 \sim \sigma_e$) up to 10^5. As the small-scale reconnection events continuously occur, electrons can be continually accelerated so the so-called "slow cooling" regime is likely to be valid. The highly efficient acceleration may help to solve the efficiency problem in GRB models and the relativistic bulk motion may explain fast variability observed in some GRB events (Zhang & Yan 2011; Deng et al. 2015).

Theoretical analysis has shown that strong particle acceleration and/or beaming effect in the reconnection region can explain the gamma-ray Crab flares (Abdo et al. 2011; Tavani et al. 2011). Our simulation shows that reconnection is a credible process that drives both strong particle acceleration and relativistic bulk motion. The strong energy conversion from magnetic energy into the plasma kinetic energy during relativistic magnetic reconnection may also help understand the so-called σ-problem, where the energy conversion is needed for dissipating the Poynting-flux dominated flow (e.g., Coroniti 1990).

In some hadronic models, a proton spectrum with $s < 2$ may be required to model TeV blazars (Böttcher et al. 2013). Our results show that ion energy gain is comparable to the electron energy gain and most of the energy goes into a nonthermal power-law spectrum. The maximum energy of protons γ_{imax} depends on the system size and the largest gyroradius can be comparable to the system size. This suggests that magnetic reconnection can be a viable mechanism for providing energetic protons in hadronic models.

Most observed energy spectra are considerably softer than the simulated results. Moreover, the hard power-laws ($s < 2$) obtained in this and other works are only in a limited energy range. While the maximum energy of particles grows with time, the power-law break energy does not and is limited by the amount of dissipated magnetic energy $\gamma_{be} \sim (m_i/m_e)\gamma_{bi} \sim [\delta\sigma_e(2-s)]^{1/(2-s)}$, where $\delta \sim 0.2$ is the fraction of the dissipated magnetic energy channeled into each species. This poses a serious problem that has to be addressed in the future. In our earlier papers (Guo et al. 2014, 2015), we have shown that particle escape from the acceleration region could lead to a softer spectrum. Since our current simulations employ periodic systems, the acceleration tends to give the hardest spectrum. This suggests more realistic open boundary conditions (e.g., Daughton et al. 2006) that include the effect of particle escape from the simulation

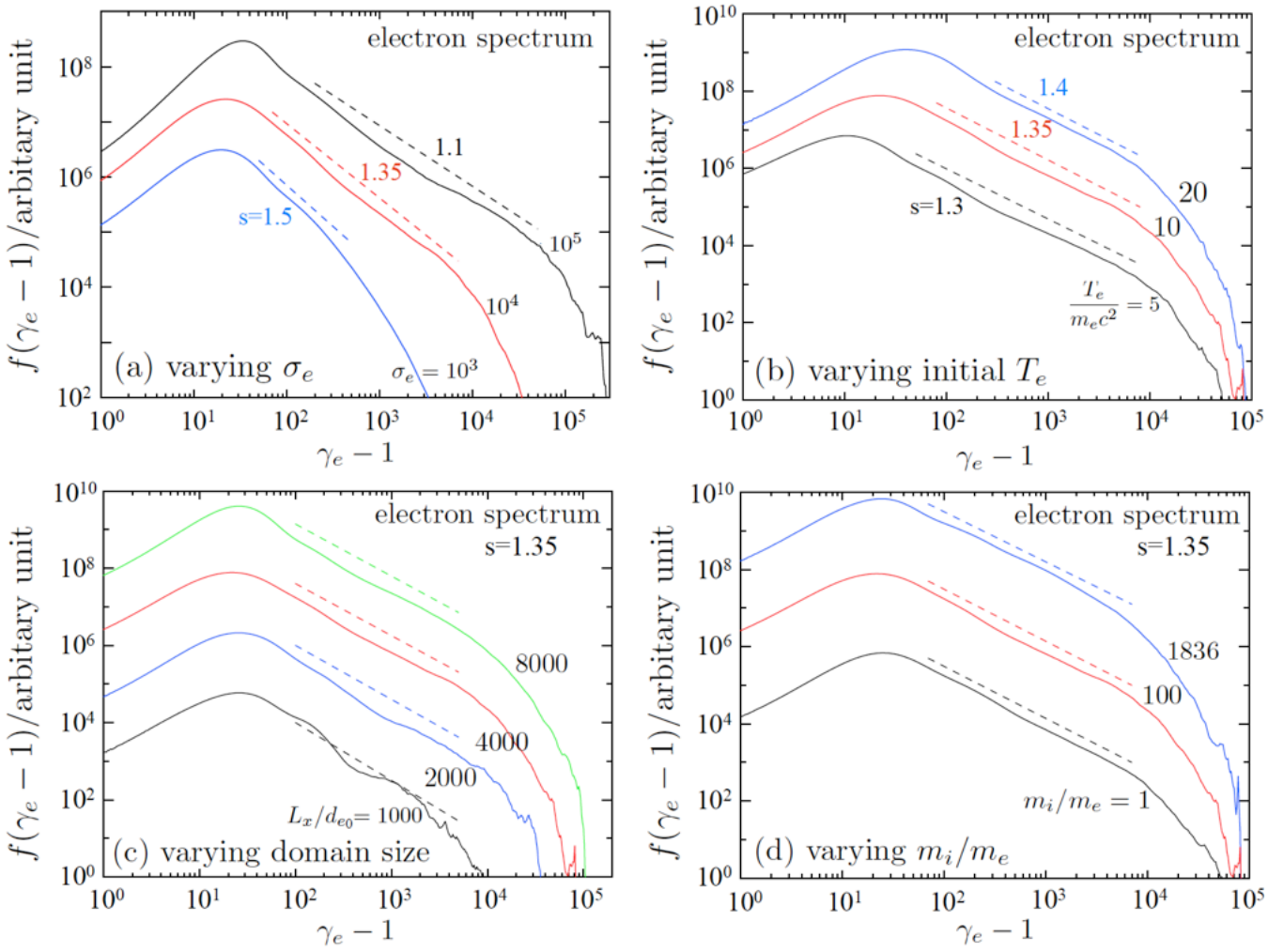

FIG. 4.— Electron energy spectra for cases with different σ_e, different temperature, different box size, different mass ratio

domain is necessary. Also, our results are tested for a domain size up to $L \sim 10^4 d_{e0}$, but for larger system the spectrum could still evolve as acceleration continues.

5. SUMMARY

Astrophysical reconnection sites have long been expected to be a strong source of nonthermal particles. Our current study has demonstrated that relativistic magnetic reconnection is efficient at generating nonthermal particles though the underlying energy conversion and acceleration process in a magnetically dominated proton-electron plasma. During reconnection, the energy distributions for both ions and electrons develop power-law spectra, which is important to understand the nonthermal emission from objects like PWNe, AGNs, and GRBs. We also find that during the active reconnection phase the outflow speeds approach the light speed and the bulk Lorentz factor can reach a few, which may help explain the observed fast variability and high luminosity emissions in several systems. These findings on plasma energization and particle acceleration in reconnection regions further demonstrate the important effect of magnetic reconnection in high-energy astrophysical systems.

ACKNOWLEDGEMENT

We are grateful to Jonathan Jara-Almonte, who developed an initial version of the particle tracking module. This work is supported by the DOE through the LDRD program at LANL and DOE/OFES support to LANL in collaboration with CMSO. X.L is supported by NASA Headquarters under the NASA Earth and Space Science Fellowship Program-Grant NNX13AM30H. Contributions from W.D. were supported by NASA from the Heliophysics Theory Program. N.L-R. is supported by the M. Hildred Blewett Fellowship of the APS. Simulation resources are provided by LANL institutional computing.

REFERENCES

Abdo, A. A., Ackermann, M., Ajello, M., et al. 2011, Science, 331, 739
Bessho, N., & Bhattacharjee, A. 2012, ApJ, 750, 129
Blackman, E. G., & Field, G. B. 1994, Physical Review Letters, 72, 494
Böttcher, M., Reimer, A., Sweeney, K., & Prakash, A. 2013, ApJ, 768, 54

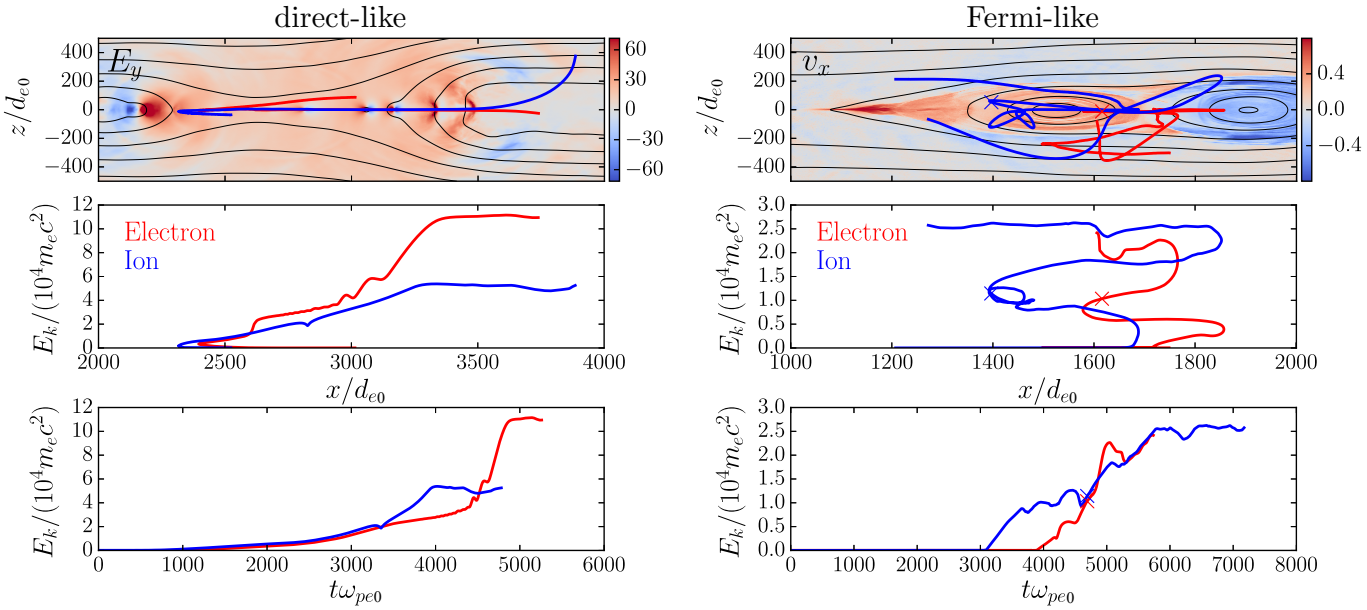

FIG. 5.— Typical trajectories for accelerated particles. Left panel shows the most accelerated particles whose trajectories similar to the direct acceleration. The color-coded contour shows the electric field in the y-direction normalized using $m_e c\omega_{pe}/e$. Right panel shows the ones typical for power-law energy range similar to the Fermi acceleration. The open circles indicate the starting points and the cross signs show the particle locations at the same time step as the field contour.

Bowers, K. J., Albright, B. J., Yin, L., et al. 2009, Journal of Physics Conference Series, 180, 012055
Cerutti, B., Uzdensky, D. A., & Begelman, M. C. 2012, ApJ, 746, 148
Comisso, L., & Asenjo, F. A. 2014, Physical Review Letters, 113, 045001
Coroniti, F. V. 1990, ApJ, 349, 538
Daigne, F., & Mochkovitch, R. 1998, MNRAS, 296, 275
Daughton, W., Scudder, J., & Karimabadi, H. 2006, Physics of Plasmas, 13, 072101
Daughton, W., & Karimabadi, H. 2007, Physics of Plasmas, 14, 072303
Deng, W., Li, H., Zhang, B., & Li, S. 2015, ApJ, 805, 163
de Gouveia dal Pino, E. M., & Lazarian, A. 2005, A&A, 441, 845
Drake, J. F., Swisdak, M., Che, H., & Shay, M. A. 2006, Nature, 443, 553
Drury, L. O. 2012, MNRAS, 422, 2474
Fu, X. R., Lu, Q. M., & Wang, S. 2006, Physics of Plasmas, 13, 012309
Giannios, D., Uzdensky, D. A., & Begelman, M. C. 2009, MNRAS, 395, L29
Guo, F., Li, H., Daughton, W., & Liu, Y.-H. 2014, Physical Review Letters, 113, 155005
Guo, F., Liu, Y.-H., Daughton, W., & Li, H. 2015, ApJ, 806, 167
Hayashida, M., Nalewajko, K., Madejski, G. M., et al. 2015, ApJ, 807, 79
Homan, D. C., Kovalev, Y. Y., Lister, M. L., et al. 2006, ApJ, 642, L115
Huang, C., Lu, Q., & Wang, S. 2010, Physics of Plasmas, 17, 072306
Kagan, D., Milosavljević, M., & Spitkovsky, A. 2013, ApJ, 774, 41
Kumar, P., & Crumley, P. 2015, MNRAS, 453, 1820
Li, X., Guo, F., Li, H., & Li, G. 2015, ApJL, 811, L24
Liu, W., Li, H., Yin, L., et al. 2011, Physics of Plasmas, 18, 052105
Liu, Y.-H., Guo, F., Daughton, W., Li, H., & Hesse, M. 2015, Physical Review Letters, 114, 095002
Lyutikov, M., & Uzdensky, D. 2003, ApJ, 589, 893
Makwana, K. D., Zhdankin, V., Li, H., Daughton, W., & Cattaneo, F. 2015, Physics of Plasmas, 22, 042902
McKinney, J. C., & Uzdensky, D. A. 2012, MNRAS, 419, 573
Melzani, M., Walder, R., Folini, D., Winisdoerffer, C., & Favre, J. M. 2014a, A&A, 570, A112
Melzani, M., Walder, R., Folini, D., Winisdoerffer, C., & Favre, J. M. 2014b, A&A, 570, A111
Oka, M., Phan, T.-D., Krucker, S., Fujimoto, M., & Shinohara, I. 2010, ApJ, 714, 915
Sironi, L., & Spitkovsky, A. 2014, ApJ, 783, L21
Sironi, L., Petropoulou, M., & Giannios, D. 2015, MNRAS, 450, 183
Spruit, H. C. 2010, Lecture Notes in Physics, Berlin Springer Verlag, 794, 233
Tavani, M., Bulgarelli, A., Vittorini, V., et al. 2011, Science, 331, 736
Titov, V. S., Galsgaard, K., & Neukirch, T. 2003, ApJ, 582, 1172
Uhm, Z. L., & Zhang, B. 2014, Nature Physics, 10, 351
Uzdensky, D. A., & Spitkovsky, A. 2014, ApJ, 780, 3
Werner, G. R., Uzdensky, D. A., Cerutti, B., Nalewajko, K., & Begelman, M. C. 2014, arXiv:1409.8262
Yan, D., Zhang, L., & Zhang, S.-N. 2015, arXiv:1511.00122
Yang, L., Zhang, L., He, J., et al. 2015, ApJ, 800, 111
Zank, G. P., le Roux, J. A., Webb, G. M., Dosch, A., & Khabarova, O. 2014, ApJ, 797, 28
Zenitani, S., & Hoshino, M. 2001, ApJ, 562, L63
Zenitani, S., & Hoshino, M. 2007, ApJ, 670, 702
Zhang, H., Chen, X., Böttcher, M., Guo, F., & Li, H. 2015a, ApJ, 804, 58
Zhang, H., Deng, W., Li, H., Böttcher, M. 2015, arXiv:1512.01307
Zhang, B., & Yan, H. 2011, ApJ, 726, 90
Zweibel, E. G., & Yamada, M. 2009, ARA&A, 47, 291